Development of decision support tools by model order reduction for active endovascular navigation

Arif Badrou, Arnaud Duval, Jérôme Szewczyk, Raphaël Blanc, Nicolas Tardif, Nahiene Hamila, Anthony Gravouil, Aline Bel-Brunon

To cite this version:

Arif Badrou, Arnaud Duval, Jérôme Szewczyk, Raphaël Blanc, Nicolas Tardif, et al.. Development of decision support tools by model order reduction for active endovascular navigation. 2022. hal-03858565v2

HAL Id: hal-03858565
https://hal.science/hal-03858565v2

Preprint submitted on 19 Apr 2023 (v2), last revised 4 Jan 2024 (v3)

Development of decision support tools by model order reduction for active endovascular navigation *Original article*

Arif BADROU[a], Arnaud DUVAL[a], Jérôme SZEWCZYK[b,c], Raphaël BLANC[b,d], Nicolas TARDIF[a], Nahiène HAMILA[e], Anthony GRAVOUIL[a], Aline BEL-BRUNON[a]

[a] *Univ Lyon, INSA Lyon, CNRS, LaMCoS, UMR5259, 69621 Villeurbanne, France*
[b] *BaseCamp Vascular (BCV), 75005 Paris, France*
[c] *Sorbonne Université, CNRS, INSERM, Institut des Systèmes Intelligents et de Robotique,ISIR, ISIR - AGATHE, F-75005 Paris, France*
[d] *Department of Interventional Neuroradiology, Fondation Rothschild Hospital, Paris, France*
[e] *Ecole Nationale d'Ingénieurs de Brest, ENIB, UMR CNRS 6027, IRDL, F-29200, Brest, France*

Abstract

Endovascular therapies consist in treating vascular pathologies mini-invasively by inserting long tools towards the area to treat. However, some trajectories are so-called complex (e.g. Supra-Aortic Trunks (SATs)). In order to facilitate the access to complex targets by catheterization, an active guidewire made of Shape Memory Alloy has been developed. Our study focuses on the navigation of this device and associated catheters towards neurovascular targets through the left carotid artery. In a previous study, a finite element model was developed to simulate the navigation of the active guidewire and catheters from the aortic arch to the hooking of the left carotid artery of

---

*Corresponding author: Aline Bel-Brunon

Email address: `aline.bel-brunon@insa-lyon.fr` (Aline BEL-BRUNON)

Preprint submitted to Journal of Theoretical, Computational and Applied Mechanics March 26, 2023

patient-specific aortas. However, numerical simulations are time-consuming and cannot be used directly in the clinic routine to provide navigation assistance. We present in this study the development of numerical charts aiming to provide a real-time computation, based on high-fidelity FE simulations, of: 1. the behaviour of the active guidewire; 2. the navigation of the active guidewire and associated catheters within a given anatomy for specific guidewire and navigation parameters. These charts are developed using the HOPGD method and demonstrate their ability to provide an accurate real-time response from a limited number of preliminary high-fidelity computations.

Keywords: Model Order Reduction, Numerical chart, Endovascular, Catheters, Guidewire, Aorta

1. Introduction

Endovascular therapies have grown significantly in the recent years. It is estimated that in 2026, 80% of cardiovascular problems will be treated by endovascular therapies [1]. The first step to treat endovascular pathologies is to reach the pathologies area. However, clinicians may be confronted to so-called complex pathways (e.g. renal arteries or Supra-Aortic Trunks (SATs)). It is estimated that 20% endovascular therapies present these complexities which may jeopardize the intervention [2]. In order to facilitate the access to complex targets through catheterization, the French company BaseCamp Vascular (BCV) developed an active guidewire made of Shape Memory Alloy, which distal tip can bend under an electric impulse. This guidewire can include several active modules; for instance for 2 modules placed in opposite directions, the guidewire tip can take an S-shape.

Our work focuses on the access to neurovascular pathologies through the left carotid artery using the active guidewire and associated catheters. Access to cerebral targets is facilitated using the active guidewire but two challenges remain for a given anatomy: (i) to optimize the design of the active guidewire by assessing the number of required actuators and their respective curvature and (ii) to propose navigation sequences maximizing the chances of reaching the target. A Finite Element (FE) model was developed to simulate the navigation of the active guidewire and catheters from the aortic arch to the left carotid artery in patient-specific aortas [3]. The numerical model offers the possibility to test particular guidewire configurations and navigation sequences.

However, numerical simulations are time-consuming and cannot be used directly in clinical routine to provide navigation assistance. An alternative is to develop numerical charts to explore in a continuous way a wide range of parameters for a limited computational cost.

Numerical charts are built using Model Order Reduction (MOR) techniques. Two families of MOR are commonly used. The methods known as POD (Proper Orthogonal Decomposition) require calculations in an offline phase (learning phase), further allowing reduction and online resolution in the reduced base (in real-time). In biomechanics and in particular for vascular problems, POD was used for example to process hemodynamic data [4, 5, 6] or to reduce the computational time of complex models [7]. The methods known as PGD (Proper Generalized Decomposition) based on the separation of variables, do not require upstream calculations. In particular, PGD is used for inverse problem solving: in [8], PGD was used to speed up the process of identifying conductivities of heart tissue. Other works have used PGD for computational surgery, [9, 10, 11] for example. One of the limitations of POD is that it is not adapted to non-linear problems (large strains in particular) and that the enrichment of the reduced bases can quickly become expensive for high dimensional problems and/or with relatively large parameter intervals. By considering uniform grids, the number of snapshots is exponential. For example, for a uniform grid of snapshots in a space of 8 parameters with 10 values to be considered in each direction, 10^8 finite element calculations would be required. We then speak of *curse of dimensionality.* PGD allows to overcome this problem since no snapshot is required. However, it remains an intrusive method and is therefore not adapted to the use of commercial softwares. The method used in the present study is HOPGD

(High Order Proper Generalized Decomposition) [12]. It is an a posteriori definition of PGD and has been used to produce 10D numerical charts in the context of real-time numerical simulation of welding processes [13]. We aim to build numerical charts based on our reference FE navigation model, to efficiently answer specific questions regarding device design and navigation sequences.

We first recall the main features of the huigh-fidelity numerical models used in this study, namely the guidewire model and the active endovascular navigation model. Then, HOPGD is briefly presented and the methods for the development of numerical charts are detailed. Proofs of concept of such charts ,developed to answer specific questions associated to endovascular active navigation, are presented. The results are finally discussed in a last part.

2. Methods

2.1. High fidelity models

In this section, we present the high-fidelity models used to develop the numerical charts: first the active guidewire model and second the navigation model.

2.1.1. Active guidewire

2.1.1.1. Structure.

The active guidewire is composed of a long shaft made of steel. At its extremity, a blade is attached and Nitinol wires are positioned on both sides of the blade and connected to electric wires. A handle allows to send an electric impulse to the Nitinol wires and by shape memory effect, the wires shrink causing the blade to bend [14, 15]. When two Nitinol wires are placed on each face of the blade, the distal tip of the active guidewire draws a S-shape to facilitate the endovascular navigation (see Fig.1).

2.1.1.2. Numerical model.

The model is built using Ls-Dyna (LSTC / ANSYS, USA). The active guidewire is simplified and represented as a long shaft with the blade. The Nitinol wires are placed on both sides of the blade and connected by rigid links. The guidewire is meshed with Hughes-Liu beam elements. The meshes were defined by convergence analysis and are visible in Fig.2. The constitutive law to model the mechanical behavior of the guidewire is hypoelastic and relates, in Eulerian form, the objective Jaumann derivative of the Cauchy stress tensor σ to the strain rate tensor $\mathbf{D}$ by the elasticity tensor $\mathbf{C}$ such that:

$$\sigma^{\nabla} = \mathbf{C} : \mathbf{D} \tag{1}$$

Tensor $\mathbf{C}$ can be decomposed into a spherical part $\mathbf{C}^{sph}$ and a deviatoric part $\mathbf{C}^{dev}$ such that:

$$\mathbf{C} = 3K\mathbf{C}^{sph} + 2G\mathbf{C}^{dev} \tag{2}$$

with K the bulk modulus and G the shear modulus.

The mechanical properties of the various portions of the guidewire are given Tab.1. The guidewire activation is simplified and produced by a displacement command as explained in [3].

2.1.1.3. Simulation of the guidewire activation.

Simulation of the guidewire is useful for guidewire developers to understand the guidewire performance, related to the Nitinol wires characteristics. The shaft is embedded and a temperature control is applied to both moduli for activation. The computational time for such a simulation is about 5 minutes. The output data are the displacements in 3D of the guidewire distal parts nodes (73 mm blade of the active guide) at the end of the simulation.

2.1.2. Endovascular navigation

2.1.2.1. Test bench.

The endovascular activation simulated in this work has been validated with respect to data acquired on a test bench including a phantom aorta (Fig.1). The simulation features aim to repoduce this configuration and the phenomena observed on this bench. The set-up is composed of a patient-specific aortic arch which can be changed and a fixed cylinder representing the descending aorta. The active guidewire is inserted and co-manipulated along with catheters.

2.1.2.2. Endovascular navigation model.

The numerical model simulates the endovascular navigation of the active guidewire and associated catheters in the aorta test bench. The catheters and the aorta are meshed with Belytschko-Tsay shell elements. The mechanical properties of the tools are either hypoelastic (using Eq.1) or hypoviscoelastic depending on the different areas. The hypoviscoelastic properties are modeled with the following law defined in [16]:

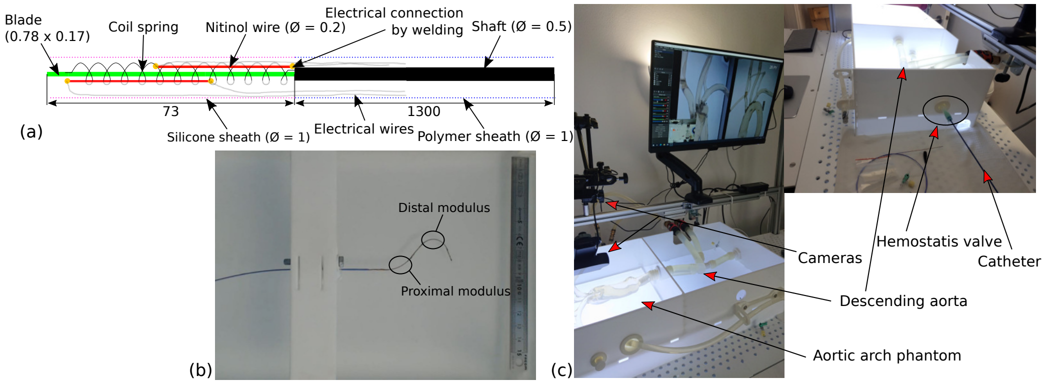

Figure 1: (a) Scheme of the active guidewire developed by BCV with two Nitinol wires placed on both sides of the blade and (b) its activation highlighting the proximal and the distal moduli. (c) Phantom aorta test bench used to test surgical tools in patient-specific aortas.

$$G(t) = G_\infty + (G_0 - G_\infty)e^{-\beta t}$$

where G_∞ and G_0 are respectively the long and short time shear moduli, parameter β is a constant expressed per time unit.

Fig.1 illustrates the tools design and dimensions as well as one aorta shell mesh. Table 1 synthetizes the tools mechanical properties, while the aorta is considered rigid. The full navigation model, involving guidewire activation but also tools translations and rotations within the aorta, was validated as described in [3] by confronting experimental navigations in patient-specific aortas to simulated ones.

The model is able to reproduce the main movements and phenomena occurring in active navigation: translations of the guidewire and the catheter, rotations of the guidewire and particular effects such as the snapping (Fig.3). Navigation sequences will be detailed later.

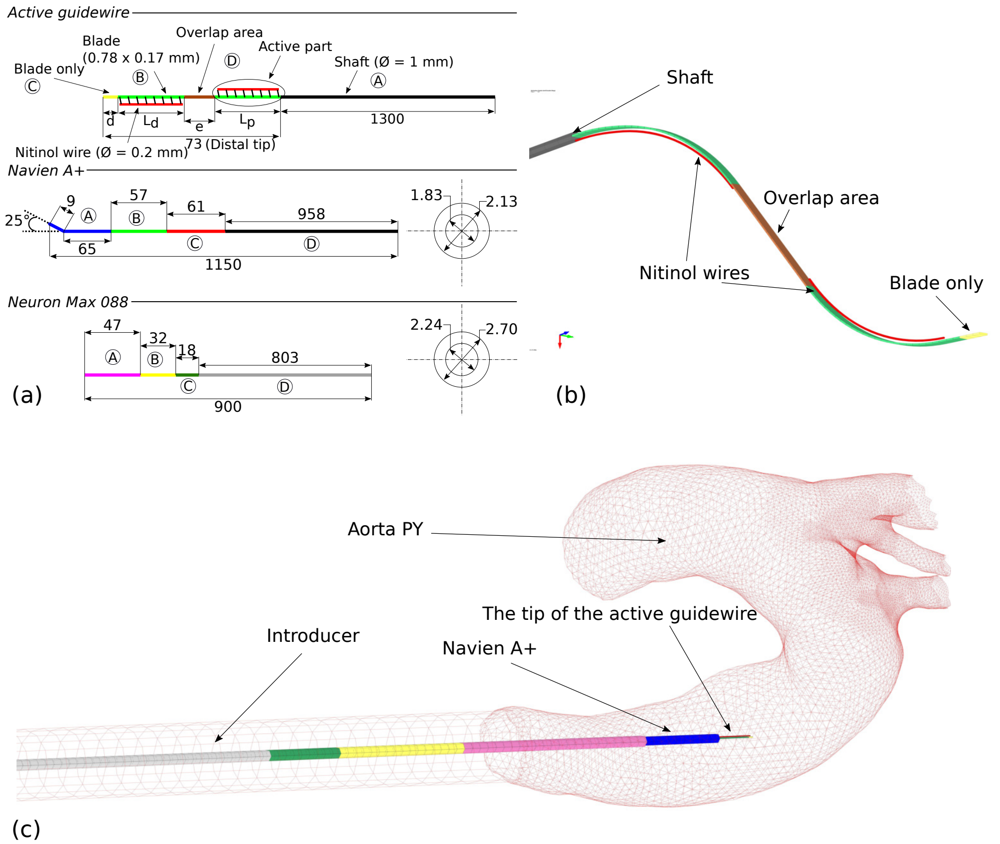

Figure 2: (a) Dimensions of the active guidewire and associated catheters. Each portion of the different tools is defined by a colour and has its own mechanical properties. (b) Activation of the device with two moduli. When the Nitinol wires are heated, they contract resulting in the S-shape bending. (c) Assembly of the different tools in the aorta. The aortic arch is a patient-specific anatomy while the descending aorta is represented by a rigid cylinder.

2.1.2.3. High fidelity simulations for the construction of decision support numerical charts.

Two numerical charts are built for the endovascular navigation in two typical aortas: the BH aorta, which is referred to as a standard aorta, and

Table 1: Mechanical properties along the surgical tools: areas A to D are related to those in Fig.2.

	A	B	C	D
Active guidewire	$E = 8047.8$ MPa $\nu = 0.3$	$E = 71130.0$ MPa $\nu = 0.3$	$E = 52720.0$ MPa $\nu = 0.3$	$E = 175000.0$ MPa $\nu = 0.3$
Navien	$\beta = 0.22\ s^{-1}$ $G_0 = 62.0$ MPa $G_\infty = 15.9$ MPa $K = 82.9$ MPa	$\beta = 0.16\ s^{-1}$ $G_0 = 94.1$ MPa $G_\infty = 26.6$ MPa $K = 152.3$ MPa	$\beta = 0.18\ s^{-1}$ $G_0 = 448.1$ MPa $G_\infty = 152.2$ MPa $K = 694.6$ MPa	$E = 1519$ MPa
Neuron	$\beta = 0.26\ s^{-1}$ $G_0 = 74.0$ MPa $G_\infty = 17.0$ MPa $K = 122.1$ MPa	$E = 250$ MPa	$E = 180$ MPa	$E = 1701$ MPa

the FM aorta, which includes a bovine arch (the left carotid artery and the brachio-cephalic trunk share the same origin). The key steps of active navigation into these aortas are illustrated Fig.4.

The distal modulus is systematically activated at the beginning of navigation to follow the shape of the arch and prevent the guidewire from entering the left subclavian artery. Therefore, the time of activation of the distal modulus is not a parameter. The output data recorded are the displacements of the guidewire distal part (73 mm blade) over time. The data are saved every 0.01s of the simulation over a total simulation time of 10.6s and 11.5s for the BH and FM aorta, respectively. Using two 2.30 GHz Xeon cores, the duration of a simulation is about 3h.

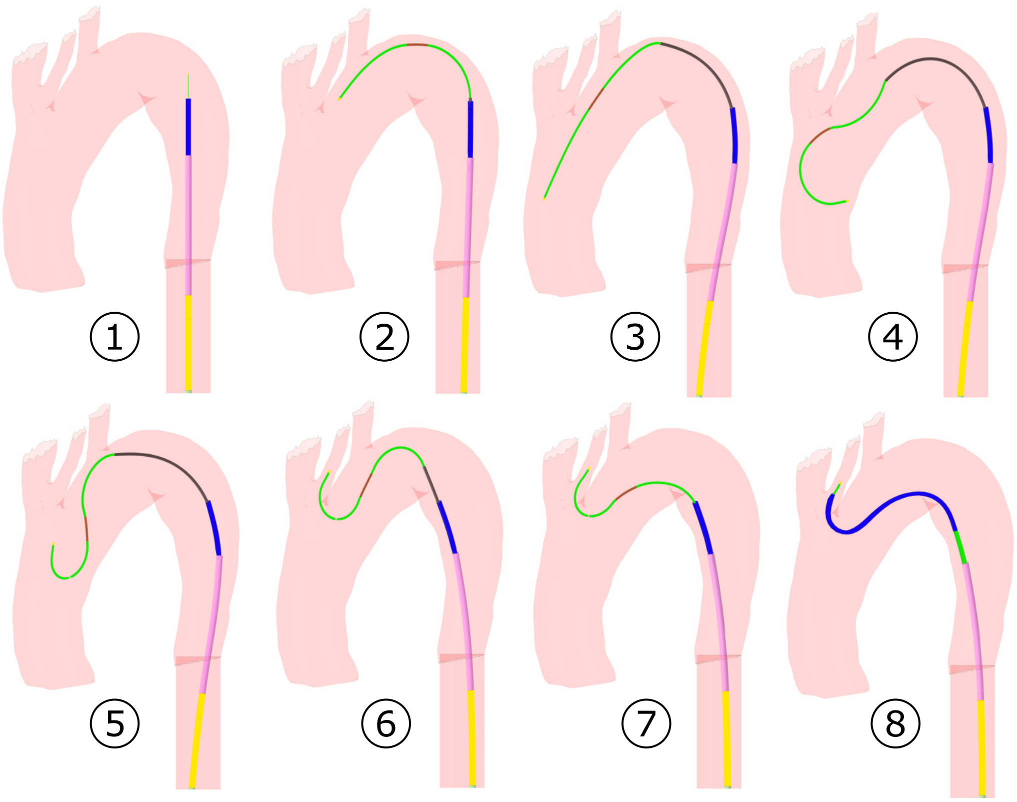

Figure 3: From ① to ③ the guidewire is initially pushed near the left carotid artery entrance. The two modules are activated in ④ while a rotation gesture is applied at the end of the active guidewire. As a consequence, the snapping effect appears(⑤) allowing to point the distal part of the guidewire in the desired direction and to stabilize the device. The guidewire is pulled from ⑥ to ⑦ to straighten the catheters with a deactivation of the proximal module to further tension it. Finally, the catheter slides over the guidewire until it reaches the left carotid artery in ⑧.

2.2. Development of numerical charts using reduced order modeling

Now that the high-fidelity FE models have been presented, the HOPGD method used to build the numerical charts is presented. A focus is proposed on the choice of the parameters of interest in this work, as it is a critical step.

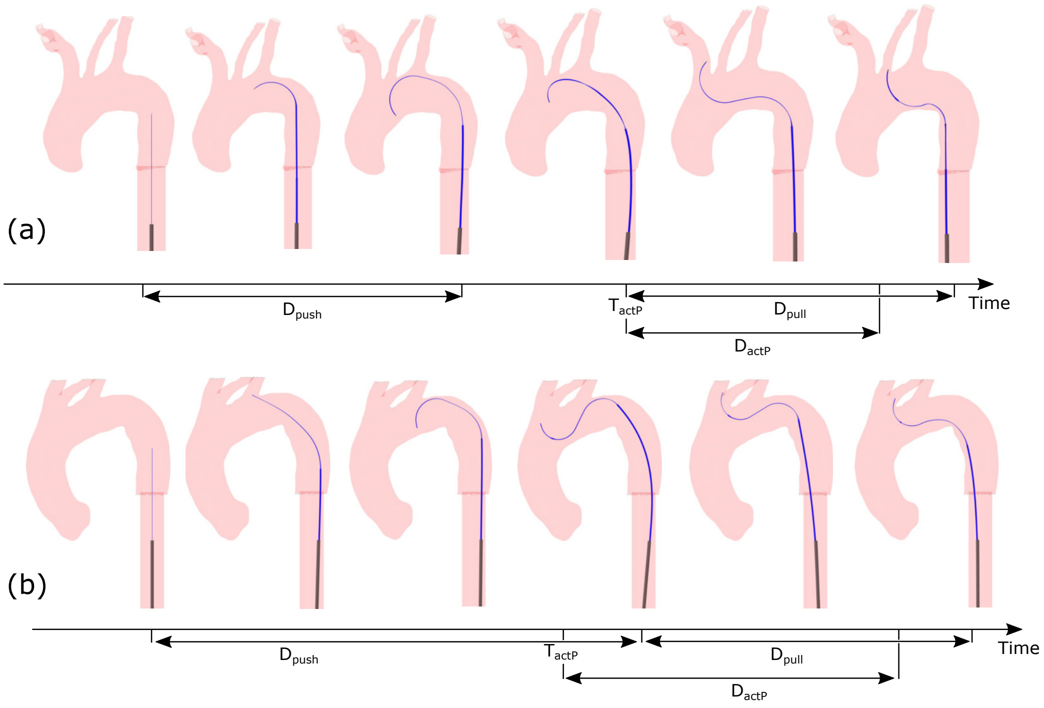

Figure 4: (a) Proposed navigation key steps for BH aorta hooking (standard aorta). The guidewire is pushed (during D_{push}) and the distal modulus is activated to prevent the device from inserting into the subclavian artery. After the guidewire is pushed, the proximal modulus is activated (at T_{actP} and during D_{actP}) and the snapping is initiated. The guidewire is then pulled (during D_{pull}). (b) The steps for navigation in the FM aorta (aorta with bovine arch) slightly differ: the guidewire navigates until it reaches the TSAs, the distal modulus is activated and snapping is triggered. The proximal modulus is then deactivated while pulling the guidewire to attempt to hook the carotid artery. Below each figure, navigation parameters driving the navigation are indicated on an axis representing time.

Then, two types of numerical charts are developed as proofs of concept: an active guidewire design tool focusing on design parameters and navigation assistance tools mixing design and navigation parameters. For each type of numerical chart, the parameter space and the snapshot selection method are presented. An error is finally calculated to evaluate the chart accuracy.

2.2.1. Methods

2.2.1.1. HOPGD.

We consider a function u dependent on parameters $p_{i=1,d}$ which can be time, space or control parameters of the problem. These parameters are assimilated to extra-coordinates of the solution and discretized in the parameter space. For each set of parameters, HOPGD seeks an approximate form u^n of u such that:

$$u(p_1, ..., p_d) \approx u^n(p_1, ..., p_d) = \sum_{j=1}^{n} \prod_{i=1}^{d} F_i^j(p_i) \tag{3}$$

n is the order of approximation and the functions $F^j_{i=1,d}$ are related to the j-th mode. These functions are determined by solving the minimization problem which consists in finding $u^n \in V_n \subset \mathcal{L}^2(\Omega)$ minimizing the cost function J such that:

$$J(u^n) = \min_{u^n \in V_n} \left(\frac{1}{2} \mid\mid u^n - u \mid\mid^2_{\mathcal{L}^2(\Omega)} \right) \tag{4}$$

This minimization problem can be solved by an alternating fixed point algorithm. For a new set of parameters, the new functions F_i are linearly interpolated from the existing functions. In this study, the version of the HOPGD algorithm does not use snapshot selection by *sparse grids* method as introduced in [17]. Thus, parameters discretization is conducted using uniform grids. Fig.5 illustrates the general procedure of the HOPGD method.

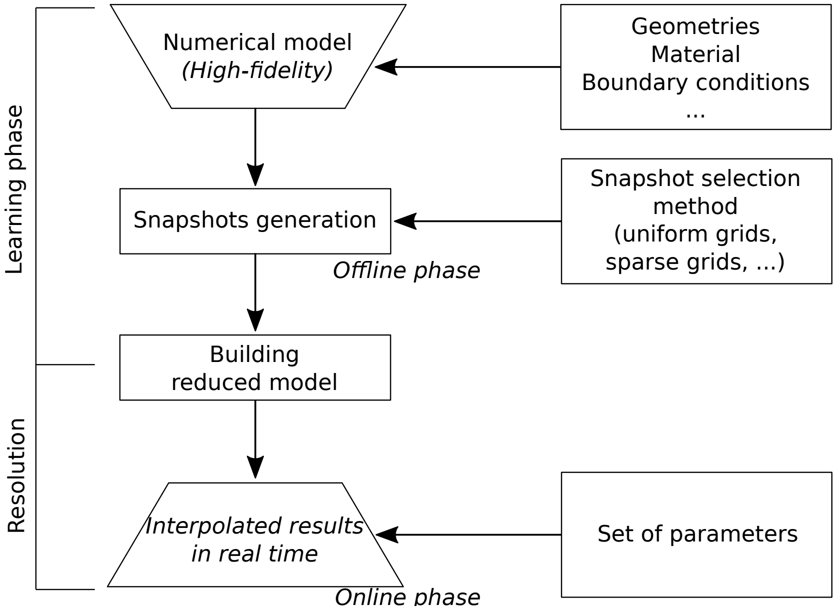

Figure 5: General procedure of the HOPGD method: starting from a high-fidelity numerical model, n parameters are considered among the geometry, material and boundary conditions. Then, the parameter space defined by the n axes is discretized using a snpashot selection method. For an uniform grid, m snapshots are selected along the axes forming a total of m^n snapshots. These snapshots are used to build the reduced model. Considering a new set of parameter within the parameter space, the HOPGD model is capable of providing a real-time response.

2.2.1.2. Error evaluation.

In order to evaluate the numerical charts performance, so-called evaluation points are selected in the center of the subdomains of the snapshot grid in the parameter space.

For each of these evaluation points, an additional finite element calculation is performed and the displacements of guidewire distal part nodes are stored in a reference U^{ref} matrix, containing the so-called high fidelity results. The reduced model is used to interpolate the results on this point and the obtained displacements are in turn stored in a U matrix. For the considered point, an error δ is computed such that:

$$\delta = \frac{|| U - U^{ref} ||}{|| U^{ref} ||}$$

With $|| \bullet ||$ the L_2 norm.

2.2.2. Application

Endovascular navigation involves many parameters. They can be classified into three categories: (i) those related to the design of the active guidewire (e.g., lengths of the active moduli or distance between them), (ii) the parameters related to navigation such as activation times or pushing / pulling times of the surgical tools and (iii) those dealing with geometric parameters (patient-specific aortas). In our study, we decided to work with fixed geometry, i.e. the parameters only relate to the design of the active guidewire and those related to the clinician gestures during navigation. In the following, two types of numerical charts are presented. First, an active guidewire design aid tool with five control parameters that are related to the device design is presented. This tool allows to compute the performance of the activated guidewire for a given set of parameters. Then, considering the design and navigation parameters, decision support numerical charts are also proposed with seven control parameters.

2.2.2.1. Active guidewire design tool.

This first tool aims to provide a design aid tool. From a given guidewire configuration, the tool computes in real time the deformation of the guidewire after activation of the moduli. The high-fidelity model used to generate the snapshots was presented in Section 2.1.1.3. The output of each snapshot corresponds to the distal guidewire position for a given design.

Choice of parameters

Five design parameters are selected for the development of the design support tool (Fig.6): the lengths L_p, L_d and e that are the lengths of the active moduli and the distance between them, respectively; parameters ϵ_L for the two Nitinol wires, which is the recoverable strain for the Nitinol wires in the shape memory effect loop representing the wire performances (change in current intensity or Nitinol grade for instance). Fig.6 also describes the parameter ranges.

Model of the active guidewire highlighting the design parameters (bold red)	Parameters
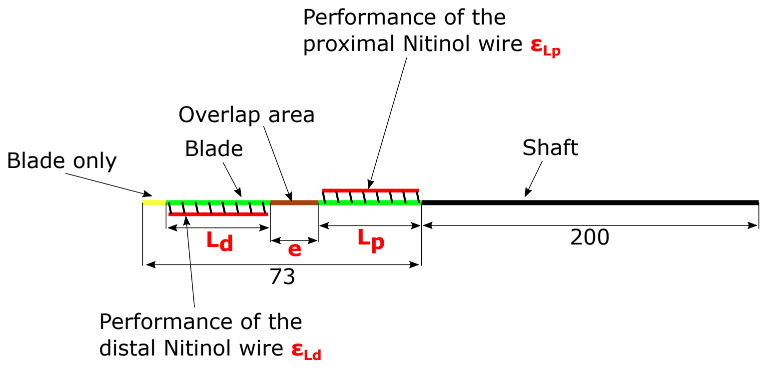	$L_p \in [15;20]$ (mm) $e \in [5;10]$ (mm) $L_d \in [15;40]$ (mm) $\varepsilon_{L_p} \in [0.01;0.0347]$ $\varepsilon_{L_d} \in [0.01;0.0347]$

Figure 6: Double stage guidewire activation model and design parameters ranges.

Snapshots selection

As previously mentioned, the version of HOPGD we use in this work does not include the sparse grids method and therefore does not allow for optimal selection of snapshots in the parameter space. Thus, it is chosen for this numerical chart to build a uniform grid with a discretization of three values per parameter (extremal values and middle of each interval), yielding a grid of $3^5 = 243$ finite element calculations to feed the HOPGD method and create the reduced model. A MatLab (MathWorks, USA) routine is used to automatically create the snapshots with the design parameters as input data. Once the snapshots are computed, the HOPGD algorithm builds the reduced model with a default number of modes fixed at 20. The reduced model is then evaluated at the center of subdomains formed by the space parameter and using the error defined Section 2.2.1.2.

2.2.2.2. Navigation assistance tools.

Introduction

In this part, more sophisticated numerical charts are proposed taking into account both design and navigation parameters. These decision support tools compute the active navigation in a given anatomy for various sets of parameters. They are proofs of concept of decision support tools which could be used in the preoperative phase. Their main advantage is the real time response. The high-fidelity model used to generate the snapshots was presented in Section 2.1.2.3.

Choice of parameters

Among the design parameters, we focused on the distal active modulus, which plays a dominant role in active navigation. Thus, parameters L_d and ϵ_{L_d} are included (Fig.6). Only the performance of the NiTi wire given by ϵ_{L_p} is selected to drive the design of the proximal modulus (L_p fixed at 27 mm and $e = 13$mm).

The other four parameters drive navigation. From a preliminary sensitivity study, the choice is made to focus on the guidewire pushing and pulling time (D_{push} and D_{pull}) and the time and duration of the activation of the proximal modulus (noted T_{actP} and D_{actP} respectively). These parameters are illustrated Fig.4. A MatLab routine was developed in this study to automatically generate the endovascular navigation models from selected parameters.

Table 2: Choice of the intervals for the seven parameters of the decision support charts. The intervals are given for the standard aorta case and with bovine arch.

Parameters	*Range of values for the standard aorta / with bovine arch*
$L_d(mm)$	[27 ; 32] / [27 ; 32]
ϵ_{L_p}	[0.026 ; 0.028] / [0.03 ; 0.033]
ϵ_{L_d}	[0.029 ; 0.033] / [0.033 ; 0.0347]
$D_{push}(s)$	[2.0 ; 3.5] / [4.2 ; 5.2]
$D_{pull}(s)$	[0.05 ; 1.5] / [1.7 ; 2.5]
$T_{actP}(s)$	[3.5 ; 4.5] / [4.7 ; 5.3]
$D_{actP}(s)$	[0.1 ; 0.6] / [1.8 ; 2.2]

Refinement and model accuracy

The accuracy of the navigation assistance tool is evaluated from an error defined, as explained in Section 2.2.1.2, as the difference between the high-fidelity model result and the reduced model result at the center of the hypercube defined by the parameter grid. However, we also propose here to dynamically improve the accuracy by adding a control loop (refinement) during the learning phase. The general procedure is visible in Fig.7.

For the construction of these numerical charts, the generation of a uniform

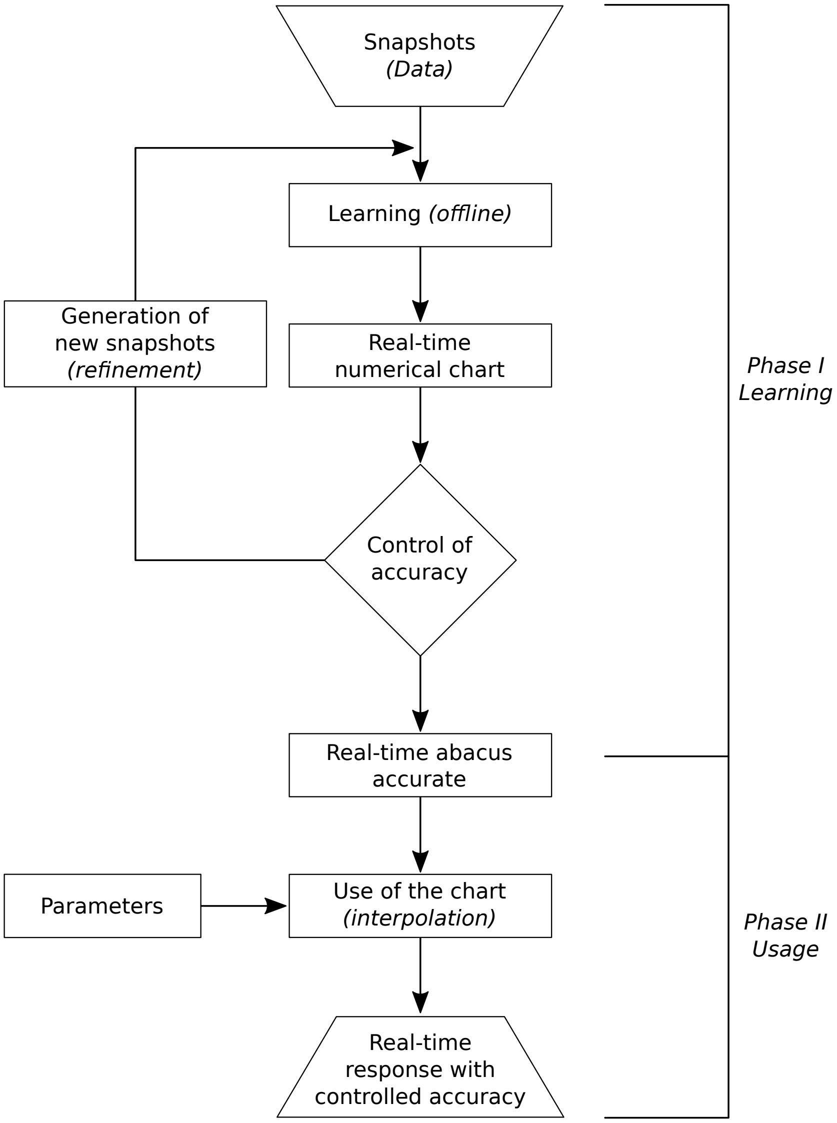

Figure 7: General procedure used for the development of decision support charts. From the snapshots computed in the parameter space in the learning phase, the reduced model is created and its accuracy is controlled. New snapshots are generated until the reduced model is considered as accurate enough. The real-time numerical chart is then used to give a real-time response given a set of parameters.

grid similar to the one used for the design aid chart (3 values per parameter) would have required $3^7 = 2187$ snapshots. A method is therefore proposed to limit the generation of many snapshots while allowing the creation of charts with a satisfactory accuracy. Fig.8. shows an overview of the process considering a 2D parameter space.

This additional procedure allows to determine the axes to be refined (requiring the addition of snapshots at the axis centers) when the error at the center of the hypercube is greater than a threshold value (here 5%). Let us note P^i the i-th parameter for $i = 1, ..., 7$, P^i_{max} the maximum value at parameter P^i (upper limit of the interval in Tab.2) and P^i_{middle} the middle of the interval of admissible values for the parameter P^i. Seven evaluation points, related to the seven parameters, are considered in order to determine which parameters most affect the error sensitivity. The first evaluation point corresponds to $\{P^1_{middle}, P^2_{max}, P^3_{max}, P^4_{max}, P^5_{max}, P^6_{max}, P^7_{max}\}$, evaluating the contribution of the first parameter. In the same way the second evaluation point corresponds to $\{P^1_{max}, P^2_{middle}, P^3_{max}, P^4_{max}, P^5_{max}, P^6_{max}, P^7_{max}\}$ and so on. The error as a function of time is then calculated for each of these evaluation points. The parameter axes associated with evaluation points whose maximum error exceeds 5% are refined by adding the midpoint on the parameter specific axis, for discretization of the snapshot grid. The procedure on a 2D case is illustrated Fig.8.

In this part, we limit ourselves to a level 1 refinement (adding only one snapshot per direction) on three axes at most, which represents a final grid of $3^3 \times 2^3 = 432$ snapshots.

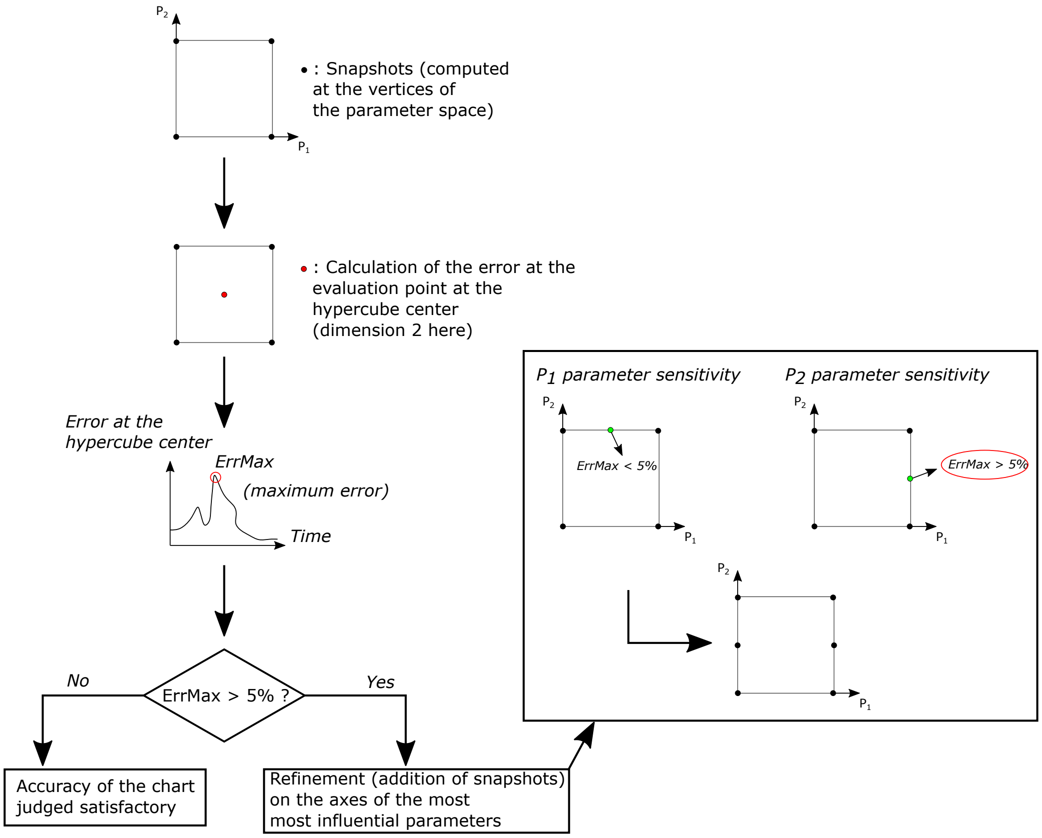

Figure 8: General procedure for the creation and refinement of decision support charts on typical aortas (learning phase in Fig.7). The first step is to perform the simulations on the parameter sets at the vertices of the grid. The error during navigation is then evaluated at the center of the hypercube. When this error exceeds a threshold fixed at 5%, the discretization in the parameter space is densified on the axes of the influential parameters (addition of snapshots at the center of these axes). Indeed, evaluation points (in green) are added at the middle of the parameter ranges to estimate sensitivity and errors are computed for both parameters. In the example, the error related to P_2 exceeds 5%. Consequently, the grid is refined to reduce the error at the hypercube center.

3. Results

3.1. Active guidewire design tool

From the 243 finite element snapshots, the reduced model is created by the HOPGD method in 17 seconds. The accuracy of the reduced model is evaluated at the different centers of the subdomains of the parameter space, i.e. on 32 evaluation points. The model is able to provide a solution in 10^{-5}s against 5 minutes for a FE calculation. The percentage errors at the different centers are given Tab.3.

The reduced model considerably decreases the computation time and allows to create the numerical chart visible on Fig.9. The graphical interface is developed with Qt Creator (Qt Group, Finland). The set of chosen parameters with the cursor interrogates the model and the interface displays the corresponding guidewire displacements.

3.2. Navigation assistance tools

3.2.1. Standard aorta

From the snapshots at the grid vertices ($2^7 = 128$ snapshots), the reduced model is created in 77 seconds. Using the method detailed in 2.2.2.2 to select the axes to be refined, values at the middle of the parameters axes of L_d, D_{pull} and T_{actP} are added, with a total number of snapshots at $3^3 \times 2^4 = 432$. The new model is built in 263 seconds and the error at the center of the hypercube is reduced. The performance, precision and parameters of the decision support tool developed are summarized in Fig.10.

3.2.2. Aorta with bovine arch

The procedure is similar for this chart applied to a bovine arch anatomy. The first model is built in 44 seconds but the error at the hypercube center required a refinement on the parameters axes of D_{pull} and T_{actP} leading to a model created in 164 seconds based on $3^2 \times 2^5 = 288$ snapshots. The errors of the model before and after refinement are displayed Fig.10 as well as the main

Table 3: Errors at the center of the subdomains of the 5 control parameters for the design aid chart.

Subdomain number	*Set of parameters*	*Error (in %)*
1	$\{15.5; 5.5; 20.5; 0.016175; 0.016175\}$	0.79
2	$\{18.5; 5.5; 20.5; 0.016175; 0.016175\}$	0.85
3	$\{15.5; 8.5; 20.5; 0.016175; 0.016175\}$	0.78
4	$\{18.5; 8.5; 20.5; 0.016175; 0.016175\}$	0.77
5	$\{15.5; 5.5; 33.5; 0.016175; 0.016175\}$	0.72
6	$\{18.5; 5.5; 33.5; 0.016175; 0.016175\}$	0.91
7	$\{15.5; 8.5; 33.5; 0.016175; 0.016175\}$	0.9
8	$\{18.5; 8.5; 33.5; 0.016175; 0.016175\}$	0.88
9	$\{15.5; 5.5; 20.5; 0.028525; 0.016175\}$	1.00
10	$\{18.5; 5.5; 20.5; 0.028525; 0.016175\}$	0.96
11	$\{15.5; 8.5; 20.5; 0.028525; 0.016175\}$	0.82
12	$\{18.5; 8.5; 20.5; 0.028525; 0.016175\}$	0.73
13	$\{15.5; 5.5; 33.5; 0.028525; 0.016175\}$	0.90
14	$\{18.5; 5.5; 20.5; 0.028525; 0.016175\}$	1.01
15	$\{15.5; 8.5; 33.5; 0.028525; 0.016175\}$	0.91
16	$\{18.5; 8.5; 33.5; 0.028525; 0.016175\}$	0.92
17	$\{15.5; 5.5; 20.5; 0.016175; 0.028525\}$	0.85
18	$\{18.5; 5.5; 20.5; 0.016175; 0.028525\}$	0.90
19	$\{15.5; 8.5; 20.5; 0.016175; 0.028525\}$	0.79
20	$\{18.5; 8.5; 20.5; 0.016175; 0.028525\}$	0.79
21	$\{15.5; 5.5; 33.5; 0.016175; 0.028525\}$	0.56
22	$\{18.5; 5.5; 33.5; 0.016175; 0.028525\}$	0.70
23	$\{15.5; 8.5; 33.5; 0.016175; 0.028525\}$	0.67
24	$\{18.5; 8.5; 33.5; 0.016175; 0.028525\}$	0.77
25	$\{15.5; 5.5; 20.5; 0.028525; 0.028525\}$	0.91
26	$\{18.5; 5.5; 20.5; 0.028525; 0.028525\}$	0.98
27	$\{15.5; 8.5; 20.5; 0.028525; 0.028525\}$	0.86
28	$\{18.5; 8.5; 20.5; 0.028525; 0.028525\}$	0.83
29	$\{15.5; 5.5; 33.5; 0.028525; 0.028525\}$	0.68
30	$\{18.5; 5.5; 33.5; 0.028525; 0.028525\}$	0.81
31	$\{15.5; 8.5; 33.5; 0.028525; 0.028525\}$	0.78
32	$\{18.5; 8.5; 33.5; 0.028525; 0.028525\}$	0.81

characteristics of this numerical chart. For the first numerical chart (standard aorta) a peak occurs at t=2s with the distal module activation. At t=5s,

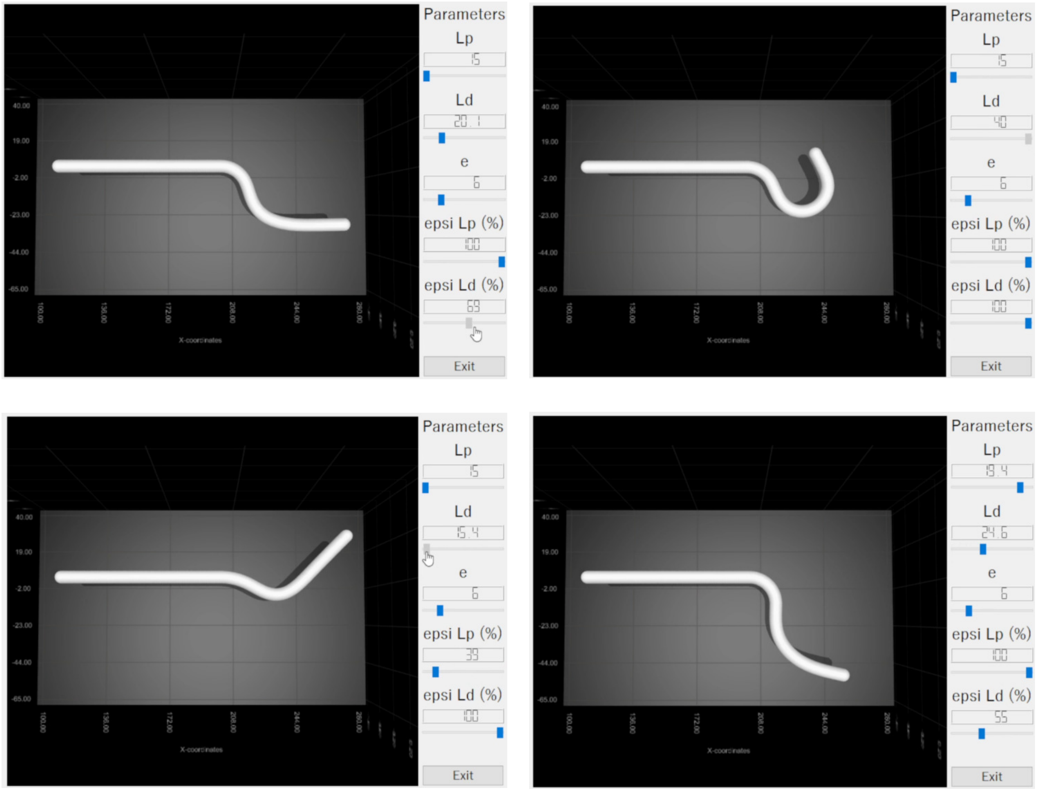

Lp 15
Ld 20.1
e 6
epsi Lp (%) 100
epsi Ld (%) 69

Lp 15
Ld 40
e 6
epsi Lp (%) 100
epsi Ld (%) 100

Lp 15
Ld 15.4
e 6
epsi Lp (%) 39
epsi Ld (%) 100

Lp 19.4
Ld 24.6
e 6
epsi Lp (%) 100
epsi Ld (%) 55

Figure 9: Numerical chart to help design the active guidewire. The five parameters can be modified and the tool allows to give a real time response of guidewire deformations with an accuracy of about 1%. A part of the rod is represented (left part of the rod) but has not been considered for the model construction. The figures represent different deformations of the guidewire according to the set of parameters defined by the user on the right panel.

snapping occurs and we can see that grid refinement highly improves the error with a better prediction of the position of the guidewire after snapping. For the second numerical chart, the error curves along time are fairly similar with a peak during snapping. At t=8.5s, grid refinement allows to better describe the position of the guidewire once pulled and the distal part abruptly hooked the aorta. The accuracy is considered satisfactory considering the relatively low number of snapshots for such a problem.

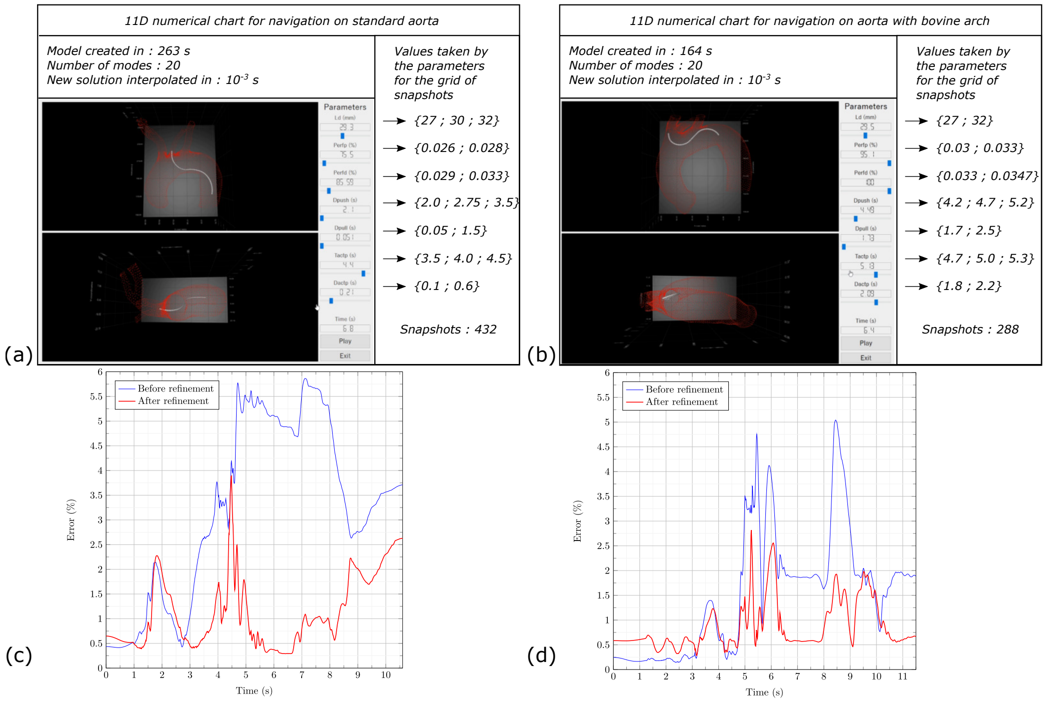

11D numerical chart for navigation on standard aorta

Model created in : 263 s
Number of modes : 20
New solution interpolated in : 10^{-3} s

Values taken by the parameters for the grid of snapshots

{27 ; 30 ; 32}
{0.026 ; 0.028}
{0.029 ; 0.033}
{2.0 ; 2.75 ; 3.5}
{0.05 ; 1.5}
{3.5 ; 4.0 ; 4.5}
{0.1 ; 0.6}

Snapshots : 432

11D numerical chart for navigation on aorta with bovine arch

Model created in : 164 s
Number of modes : 20
New solution interpolated in : 10^{-3} s

Values taken by the parameters for the grid of snapshots

{27 ; 32}
{0.03 ; 0.033}
{0.033 ; 0.0347}
{4.2 ; 4.7 ; 5.2}
{1.7 ; 2.5}
{4.7 ; 5.0 ; 5.3}
{1.8 ; 2.2}

Snapshots : 288

Figure 10: Characteristics of the numerical decision support chart on a standard aorta (a) and an aorta with bovine arch (b). In (c) and (d) the errors of the reduced model as a function of time evaluated at the hypercube center in the parameter space are displayed for the standard aorta and the aorta with bovine arch, respectively.

3.2.3. *Conclusions on decision support charts*

Overall, the charts show very satisfactory results. The snapping is correctly replayed and the contact well represented. For each new set of parameters, the tools provide an instantaneous response (10^{-3}s) compared to nearly 3 hours for a high-fidelity FE calculation. The response time of the numerical chart is well below the specifications.

Concerning the error curves in blue for the two charts (Fig.10), peaks at key stages of the navigation are observed. The first peak occurs when the distal modulus is activated. While snapping, the error increases sharply. For the first chart, this error gradually decreases and then increases again when the guidewire is pulled. The second chart error curve shows successive peaks during snapping, mainly due to guidewire high frequency vibrations. A second peak is visible when the proximal modulus is deactivated.

4. Discussion

4.1. Main results

The HOPGD method was used to build numerical charts and proved to be efficient for problems with many parameters as it was the case in this study.

A first chart has been developed to help the guidewire design optimization. Only guidewire design parameters were studied. Considering the simulation time of the snapshots used to create the reduced model and the preliminary tests, it was chosen to work on a uniform grid with three values per axis. Since the ranges were relatively wide, the errors of the reduced model were evaluated at the centers of the subdomains formed by the grid and reached 1%. A refinement was therefore not required for this chart.

Then, the objective was to work on more complex charts combining design and navigation parameters. These tools were thought of as proofs of concept of what could be achieved using model reduction methods in a biomechanical and in particular cardiovascular framework.

Some remarks about the choice of the navigation parameters and their values can be formulated: these parameters are considered to be the most influential for left carotid artery hooking. The extrema of these parameters were determined by a preliminary analysis. With these values the guidewire navigates between the origins of the left subclavian and the brachiocephalic trunk. The values do not overlap and they are associated to specific navigation sequences. Indeed, the extrema values were chosen such as the main navigation steps are the same over the snapshots: considering the navigation into the BH aorta for instance, the guidewire is first pushed, the proximale module is activated and then the guidewire is pulled. Other sequences can not be obtained with these charts.

In the context of this study, real time is of the order of a second, comparable to the reaction time when using the graphical interface. For integration of numerical chart in a medical robotics environment, we would target a response time of the order of 0.1s maximum, to be able to capture and control the fast movements of the tools. However it should be emphasized that this chart provides the navigation over time and not only the final configuration. After refinement, the error remains below 4% which can be considered as very satisfactory, especially because this maximum error occurs at snapping. We expceted this phenomenon to be much less reductible.

In general, it was interesting to test the performance of the HOPGD method in our problem associating nonlinearities, contact and fast phenomena.

4.2. Study limits

Many tests (charts with less parameters, simulations to study the sensitivity to some parameters) have been conducted beforehand and two main difficulties have been highlighted: the choice of parameters and their range of values. The active guidewire was developed during this work. As a consequence, there was not the necessary hindsight to choose, in an optimal way, the parameters to be incorporated in the chart. We then relied on the experience gained from the numerous simulations performed.

Concerning the values ranges, charts with two or three parameters allowed to show that too large ranges would require many simulations. In order to develop proofs of concept and taking into account the available resources, a maximum of 432 snapshots per chart was set. With seven control parameters, the selected value intervals were therefore quite small and did not allow to explore large variations of the guidewire navigation. The main limitation came from the use of uniform grids. It would be interesting to improve the generation of snapshots with a sparse grid method.

The errors for both decision support charts were evaluated at the center of the hypercube. An error within 5% was considered satisfactory. This criterion was determined by judging the displacements of the guidewire relative to the aorta: for the tested charts, a higher error corresponded to poor management of the contact between the guidewire and the aorta. Moreover, the peaks occured during the fast phenomena: activation and deactivation of the modules or even snapping. A solution to smoothen the curves could be to save more data as a function of time (reduction of the time step used to save the guidewire displacements) so as to better capture these phenomena. However, it would require a large amount of storage.

A method, adapted specifically for this study, allowed us to select the axes to refine the grid when this error exceeded 5%. For intervals with larger extrema, further refinements in the sub-domains may be considered.

5. Conclusion

This study presents numerical charts for design and decision support tools dedicated to the use of the active guidewire. These solutions serve as a proof of concept and show very promising results. Fixed anatomy numerical charts were proposed in this study. A more powerful tool could incorporate geometric parameters and allow, for a new patient, to provide real-time decision support.

6. Acknowledgements

The French National Research Agency (ANR) partially supported this work through the DEEP project: Devices for augmEnted Endovascular navigation in complex Pathways (grant n°ANR-18-CE19-0027-01).

7. Conflict of interest statement

The authors declare that there are no conflicts of interest.

References

[1] R. Verhage, E. Hazebroek, J. Boone, R. van Hillegersberg, Minimally invasive surgery compared to open procedures in esophagectomy for cancer: A systematic review of the literature, Minerva chirurgica 64 (2009) 135–46.

[2] S. Madhwal, V. Rajagopal, D. Bhatt, C. Bajzer, P. Whitlow, S. Kapadia, Predictors of Difficult Carotid Stenting as Determined by Aortic Arch Angiography, J. Invasive. Cardiol. 20 (2008) 200–4.

[3] A. Badrou, N. Tardif, P. Chaudet, N. Lescanne, J. Szewczyk, R. Blanc, N. Hamila, A. Gravouil, A. Bel-Brunon, Simulation of multi-curve active catheterization for endovascular navigation to complex targets, Journal of Biomechanics 140 (2022) 111147.

[4] S. Kefayati, T. L. Poepping, Transitional flow analysis in the carotid artery bifurcation by proper orthogonal decomposition and particle image velocimetry, Medical Engineering & Physics 35 (7) (2013) 898–909.

[5] G. Janiga, Quantitative assessment of 4D hemodynamics in cerebral aneurysms using proper orthogonal decomposition, Journal of Biomechanics 82 (2019) 80–86.

[6] A. Darwish, G. Di Labbio, W. Saleh, L. Kadem, Proper Orthogonal Decomposition Analysis of the Flow Downstream of a Dysfunctional Bileaflet Mechanical Aortic Valve, Cardiovascular Engineering and Technology 12 (3) (2021) 286–299.

[7] R. R. Rama, S. Skatulla, C. Sansour, Real-time modelling of diastolic filling of the heart using the proper orthogonal decomposition with interpolation, International Journal of Solids and Structures 96 (2016) 409–422.

[8] A. Barone, M. G. Carlino, A. Gizzi, S. Perotto, A. Veneziani, Efficient estimation of cardiac conductivities: A proper generalized decomposition approach, Journal of Computational Physics 423 (2020) 109810.

[9] C. Quesada, D. González, I. Alfaro, E. Cueto, F. Chinesta, Computational vademecums for real-time simulation of surgical cutting in haptic

environments, International Journal for Numerical Methods in Engineering 108 (10) (2016) 1230–1247.

[10] C. Quesada, I. Alfaro, D. González, F. Chinesta, E. Cueto, Haptic simulation of tissue tearing during surgery, International Journal for Numerical Methods in Biomedical Engineering 34 (3) (2018) e2926.

[11] S. Niroomandi, D. González, I. Alfaro, F. Bordeu, A. Leygue, E. Cueto, F. Chinesta, Real-time simulation of biological soft tissues: a PGD approach, International Journal for Numerical Methods in Biomedical Engineering 29 (5) (2013) 586–600.

[12] D. Modesto, S. Zlotnik, A. Huerta, Proper generalized decomposition for parameterized Helmholtz problems in heterogeneous and unbounded domains: Application to harbor agitation, Computer Methods in Applied Mechanics and Engineering 295 (2015) 127–149.

[13] Y. Lu, N. Blal, A. Gravouil, Multi-parametric space-time computational vademecum for parametric studies: Application to real time welding simulations, Finite Elements in Analysis and Design 139 (2018) 62–72.

[14] D. C. Lagoudas, Shape Memory Alloys, Vol. 1, Springer US, Boston, MA, 2008.

[15] T. Couture, J. Szewczyk, Design and Experimental Validation of an Active Catheter for Endovascular Navigation, Journal of Medical Devices 12 (Nov. 2017).

[16] L. R. Herrmann, F. E. Peterson, A Numerical Procedure for Viscoelastic Stress Analysis, Orlando, Fl., 1968.

[17] Y. Lu, N. Blal, A. Gravouil, Adaptive sparse grid based HOPGD: Toward a nonintrusive strategy for constructing space-time welding computational vademecum, International Journal for Numerical Methods in Engineering 114 (13) (2018) 1438–1461.